PCCP

Electronic Structure Analysis and DFT Benchmarking of Rydberg-type Alkali-Metal-Crown Ether, -Cryptand, and -Adamanzane Complexes

Journal:	*Physical Chemistry Chemical Physics*
Manuscript ID	CP-ART-02-2024-000723.R1
Article Type:	Paper
Date Submitted by the Author:	31-Mar-2024
Complete List of Authors:	Ariyarathna, Isuru; Los Alamos National Laboratory

Electronic Structure Analysis and DFT Benchmarking of Rydberg-type Alkali-Metal-Crown Ether, -Cryptand, and -Adamanzane Complexes

Isuru R. Ariyarathna

Physics and Chemistry of Materials (T-1), Los Alamos National Laboratory, Los Alamos, NM 87545, USA

Email: isuru@lanl.gov

Abstract

Density functional theory (DFT) and electron propagator theory (EPT) calculations were performed to study ground and excited electronic structures of alkali-metal (M) coordinated 9-Crown-3, 24-Crown-8, [2.1.1]Cryptand, *o*-Me_2-1.1.1, and 3^6Adamanzane complexes. Each complex bears an expanded electron in the periphery and occupies diffuse 1p-, 1d-, 1f-type molecular orbitals (or superatomic 1P, 1D, 1F orbitals) in excited electronic states. The calculated superatomic shell model of the M(9-Crown)$_2$ is 1S, 1P, 1D, 1F, 2S, 2P, 2D, 1G and it is held by all other complexes up to the studied 1F level. Due to the highly diffuse nature of the electron, the ionization energies of these complexes are significantly lower (1.6-2.0 eV) and belong to the superalkali category. The *ab initio* EPT ionization energy and the excitation energies of the Li(9-Crown)$_2$ were used to evaluate DFT errors associated with a series of exchange correlation functionals that span multiple rungs of Jacob's ladder (i.e., GGA, meta-GGA, global GGA hybrid, meta-GGA hybrid, range-separated hybrid, double-hybrid). Among these, the best performing functional is the range-separated hybrid CAM-B3LYP and the errors are within 6% of high-level *ab initio* EPT results. The accuracy of CAM-B3LYP is indeed transferable to similar complexes and hence the findings are expected to accelerate the progression of studies of Rydberg-type systems.

I. Introduction

Atom and molecule encapsulated macromolecules or molecular cages often possess unique physicochemical properties compared to their isolated fragments.[1-6] In this regard, development and structural modification of metal-encapsulable macrocyclic ligands for achieving the desired host-guest environments is an ongoing effort especially due to their potential applications in medicine, catalysis, and material science.[5-11] Macrocyclic-polyethers and -polyamines are ideal hosts for the encapsulation of metal atoms. Their electron rich O- and N-coordination-sites provide a greater inertness for metal cations with stabilized low oxidation states.[12] Interestingly, with such electron rich coordinating sites and their chelating effects, the ligand (L) can be powerful enough to force valence electrons out of the encapsulating metal atom (M) to the periphery.[13, 14] This produces Rydberg-type complexes with an ionic $(ML)^{q+}@qe^-$ structure (q = number of peripheral or diffuse electrons). For example, the alkali-metal coordinated saturated crown-ethers, cryptands, and their aza analogues bear greatly diffuse electrons in the vicinity of the ligand.[15, 16] In these cases, the central metal cation is highly stabilized (and not electron deficient), and hence its attraction to the diffuse electron is weaker endowing the complexes with lower ionization energies (IEs).[4, 14, 15] Several such alkali-metal crown ethers and cryptand complexes carry lesser IEs than alkali-metal atoms (or explicitly lower IEs than the IE of Cs-atom, i.e., 3.89 eV) and have been identified as "superalkalis".[14, 17] Specifically, the lowest IE reported until now is for the K[2.2.2]cryptand complex which is 1.52 eV.[14] Such systems with lower IEs are indeed excellent reducing agents and are also mooted as efficient catalysts.[18, 19]

The diffuse electron cloud of some of these diffuse complexes, i.e., Na(15-Crown-5), K(18-Crown-6), M[2.2.2]Cryptand, $M(Tren)_2$, M(Azacryptand), M(TriPip222) for M = Na and K, is quasispherical in nature (like an s-orbital) and intriguingly, it populates higher angular momentum p-, d-, f-, and g-type orbitals in excited states.[15, 16, 20] Owing to this singularity, in the past we identified such complexes as "superatoms" and with excited state analysis, their superatomic (SA) Aufbau principle was disclosed to be 1S, 1P, 1D, 1F, 2S, 2P, and 1G (for some complexes, the 2S orbital populate prior to 1F).[15, 16] It is interesting to note that this SA orbital order resembles the "Jellium shell model" ($1s^21p^61d^{10}2s^21f^{14}2p^61g^{18}2d^{10}3s^21h^{22}2f^{14}3p^6$...) of metal clusters.[21] Similar shell models have been observed for several Rydberg-type alkali-metal or mono-cationic alkaline earth metal coordinated ammine, aqua, and hydrogenated fullerene species as well, i.e., $M(NH_3)_4$ (M = Li, Na, Be^+)[22, 23], $M(H_2O)_6$ (M = Mg^+, Ca^+)[24, 25], and $M@C_{20}H_{20}$ (M = Li, Na, K, Rb, Mg^+, Ca^+)[1, 2]. It should be noted that the accurate computational analysis of the excited states of such systems is rather challenging due to the extensively diffuse nature of the peripheral electron which requires the implementation of high-level

of quantum chemical methods with highly diffuse basis sets.[26-32] This could be the major reason for the scarcity of excited state studies available on such systems in the literature.

The present work is a much-needed extension to our ongoing attempts to analyze electronic structures of molecules with diffuse electrons.[1, 2, 15, 22-25, 27, 30, 33] Here ground and excited electronic states of several such alkali-metal (M) coordinated crown ether (i.e., 9-Crown-3 and 24-Crown-8), cryptand (i.e., [2.1.1]Cryptand and orthoester cryptand *o*-Me_2-1.1.1), and 3^6Adamanzane (3^6Adz) complexes are investigated by means of high-level quantum calculations. Note that these complexes, their charged species, or their derivatives have been the focal point of several theoretical and/or experimental studies (see Refs. 14, 34-41). To provide a better understanding of these fascinating species' properties (i.e., SA shell models, excitation energies, and ionization energies), a thorough comparison is made with similar Rydberg-type complexes reported in the literature. Furthermore, trends that contribute to lower IEs and excitation energies that could be used for their property tuning by structural modifications are also explored. To promote further studies on similar systems, a part of this work is devoted to DFT (density functional theory) benchmarked by probing several exchange-correlation functionals that span multiple rungs of ''Jacob's ladder''[42] (i.e., GGA, meta-GGA, global GGA hybrid, meta-GGA hybrid, range-separated hybrid, and double-hybrid). Specifically, the functional errors associated with the ionization energies and excitation energies are assessed. Finally, the gained DFT knowledge is exploited to predict more accurate ionization energies and excitation energies of several larger Rydberg-type complexes.

II. Computational details

The geometries of all reported complexes were optimized at the previously benchmarked DFT/CAM-B3LYP level.[30] Correlation-consistent triple-ζ quality cc-pVTZ (M, C, N, O) aug-cc-pVTZ (H) basis set was used for the geometry optimizations of M(9-Crown-3)$_{n=1,2}$ and M[2.1.1]Cryptand, whereas geometries of all other species were optimized at the double-ζ quality cc-pVDZ (M, C, N, O) aug-cc-pVDZ (H) basis set.[43-46] At the same level of theory, the dissociation energies (D_es) of all complexes were calculated with respect to the $M(L)_n \rightarrow M + nL$ fragmentation when all fragments are at their ground electronic state (L = chelating ligand, n =1, 2). The Cartesian coordinates of the optimized CAM-B3LYP geometries and B3LYP harmonic vibrational frequencies are listed in the Electronic Supporting Information (ESI Tables S1-S11). Note that to obtain B3LYP frequencies, all geometries were reoptimized at B3LYP level using the same basis sets. This approach was utilized since the CAM-B3LYP frequency calculations are substantially time-consuming compared to B3LYP frequency calculations.

Excited states were studied utilizing the electron propagator theory (EPT). The Koopmans' theorem (KT), diagonal second-order (D2), partial third-order quasiparticle (P3), and renormalized partial third-order quasiparticle (P3+) EPT methods were applied to calculate vertical electron attachment energies (VEAEs) of M(9-Crown-3)$_2^+$ and M[2.1.1]Cryptand$^+$.[47-51] The VEAEs of M(*o*-Me$_2$-1.1.1)$^+$, M(24-Crown-8)$^+$, and Li[3^{6}Adz]$^+$ were calculated only at the D2 level to minimize the associated higher computational cost. In each case, the differences of the EPT VEAEs were used to infer excitation energies of the neutral complexes (see Refs. 49-51 for more information). For all EPT calculations CAM-B3LYP geometries of the neutral complexes were used. Note that the cost and the accuracy of the EPT calculations vary in the order of KT < D2 < P3 < P3+. All pole strengths corresponding to the VEAEs are greater than 0.85 and hence the EPT results are reliable (the VEAEs and corresponding pole strengths are reported in the ESI Tables S13, S15, S17, S19, S21, S23, S25, S27, and S29). All EPT calculations were performed with the previously benchmarked cc-pVDZ (M, C, N, O) d-aug-cc-pVDZ (H) basis set combination.[23, 24, 30]

Single-point DFT calculations were performed for Li(9-Crown-3)$_2$ and Li(9-Crown-3)$_2^+$ at a series of exchange-correlation functionals that span multiple rungs of Jacob's ladder[42] (i.e., GGA, meta-GGA, global GGA hybrid, meta-GGA hybrid, range-separated hybrid, double-hybrid) to access DFT errors associated with VIEs. For TD-DFT (time-dependent DFT) calculations of Li(9-Crown-3)$_2$ all aforementioned functionals except for the double-hybrids were utilized. CAM-B3LYP optimized geometries of Li(9-Crown-3)$_2$, K[2.2.2]Cryptand, methylated-K[2.2.2]Cryptand, and ethylated-K[2.2.2]Cryptand were used for the DFT VIE and TD-DFT benchmark calculations with the cc-pVDZ (M, C, N, O) d-aug-cc-pVDZ (H) basis set.

Gaussian 16 software was used for all DFT and EPT calculations.[52] IboView[53], Avogadro[54, 55], and Molden[56] software packages were used for structures and molecular orbitals visualizations.

III. Results and discussion

III.A. *Ab initio* analysis of M(9-Crown-3)$_{n=1,2}$, M[2.1.1]Cryptand, M(*o*-Me$_2$-1.1.1), M(24-Crown-8), and M(3^{6}Adz) (M = Li, Na, K)

The nature of the ligand environment and a specific number of ligand units are vital for the origination of a Rydberg-type molecule. For example, a 9-Crown-3 is incapable of displacing a ns^1 electron of an alkali-metal atom (M) to the ligand periphery to create such a system where the radical electron would rather localize at the M with a significant polarization away from the ligand (ESI Figure S1). However, the reaction of M with two 9-Crown-3 ligands displaces its valence ns^1 electron

to the periphery creating a Rydberg-type complex, i.e., M(9-Crown-3)$_2$ (Figure 1 and ESI Figure S1). Such systems with diffuse electrons are also known as "surface-type" complexes.[57, 58] Similar to the M(9-Crown-3)$_2$, all M[2.1.1]Cryptand, M(*o*-Me$_2$-1.1.1), M(24-Crown-8), and M(3^{6}Adz) (M = Li, Na, K) systems pursued in this work carry diffuse electrons in the periphery (Figure 1 and ESI Figure S1). Notice that these extended electron clouds of each surface-type complexes are quasispherical mimicking an s-orbital (ESI Figure S1). Indeed, the diffuse electron(s) of such complexes are known to govern some of their geometrical parameters. For example, the attraction of δ^+ charged H-atoms towards the exterior electron cloud elongates the C–H bonds, while the repulsion between the δ^- O/N centers and the diffuse electron contracts the M–O or M–N bonds.[1, 15, 23] These patterns are preserved by several complexes studied in this work, i.e., longer C–H and shorter M–O/N bonds compared to their cations (ESI Table S30). But the trend is not maintained for a few M–O bonds of the Li[2.1.1]Cryptand and M(24-Crown-8) complexes (compare the bond lengths in ESI Table S30).

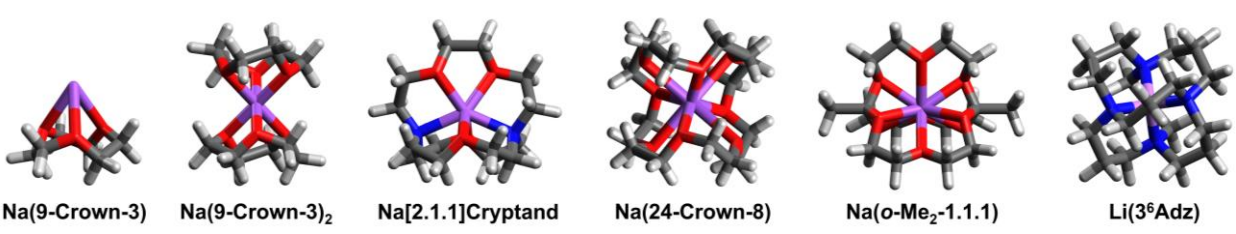

Figure 1. Geometries of Na(9-Crown-3)$_{n=1,2}$, Na[2.1.1]Cryptand, Na(24-Crown-8), Na(*o*-Me$_2$-1.1.1), and Li(3^{6}Adz) complexes. Their corresponding Li- or K-complexes have similar shapes.

In the past we have seen that the D_es of such complexes depend on the compatibility between the sizes of the encapsulating M atom vs. the ring cavity of the ligand.[15, 16, 20] Furthermore, when M moves from top-to-bottom of the column of the periodic table, a gradual decrease of D_es is expected. In harmony with the available literature, the studied Li-complexes carry larger D_es compared to corresponding Na-complexes (Table 1). Similarly, the heavier K(24-Crown-8) has a smaller D_e compared to the lighter Na(24-Crown-8). The largest D_e differences were observed for the M(9-Crown-3)$_2$ and M[2.1.1]Cryptand, where the D_es of Li-complexes are 3-4 times greater compared to their Na-complexes. Among the studied complexes the highest D_e was observed for the Li[2.1.1]Cryptand, which is 41.9 kcal/mol.

The surface-type M-ligand complexes are expected to carry lower ionization potentials due to the weaker interaction between the ML_n^+ core and the diffuse electron. This is clearly demonstrated by the lower VIEs of the surface-type Li(9-Crown-3)$_2$ compared to the "valence-type"[57, 58] Li(9-Crown-3), i.e., 1.901 vs. 2.944 eV (P3+ VIE of Table 1). Indeed, this difference is greater (by 1.4 eV) for Na(9-

Crown-3) vs. Na(9-Crown-3)$_2$ (Table 1). The expensive P3 and P3+ EPT VIE calculations are only performed for the M(9-Crown-3)$_{n=1,2}$ and M[2.1.1]Cryptand complexes, whereas EPT VIEs of larger M(*o*-Me$_2$-1.1.1), M(24-Crown-8), and Li(3^{6}Adz) were obtained at the comparatively less expensive D2 level. The D2 values are indeed reliable and are nearly identical to our highest level of theory (P3+) values. Specifically, the discrepancies between D2 and P3+ VIEs are less than 0.01 eV (Table 1). Among all surface-type species, the Na-complexes possess lower VIEs compared to the corresponding Li-complexes (by 0.01-0.07 eV) except for the M(*o*-Me$_2$-1.1.1) where it is the opposite, but only by 0.001 eV (Table 1). This slightly higher VIE of Na(*o*-Me$_2$-1.1.1) compared to the Li(*o*-Me$_2$-1.1.1) may have been caused by the size incompatibility of the latter compared to the former. Specifically, the Li-atom is stabilized by sliding to one side of the *o*-Me$_2$-1.1.1 cavity with C_1 symmetry rather than settling at the center with C_{3h} symmetry (ESI Figure S2). Note that the C_1 structure is stabilized by 2.6 kcal/mol over the C_{3h} structure at the DFT/B3LYP level. Indeed, this energy difference is significant and the properties calculated under the C_{3h} symmetry would not perfectly translate to the properties obtained at the C_1 structure. The EPT calculations of Li(*o*-Me$_2$-1.1.1) with the C_1 symmetry is computationally rather challenging and only the first excitation energy under D2 level was calculated (i.e., 0.310 eV). Comparatively, the first excited state under the C_{3h} geometry lies 0.157 eV (or 3.6 kcal/mol) lower in energy. Although these excitation energies (at C_{3h} vs. C_1 geometries) are somewhat different, the excitation energies and the shell models calculated under C_{3h} symmetry could be utilized to make comparisons with similar Rydberg-type systems.

The gradual decrease of VIE moving from Li-to-Na- or Na-to-K-based surface-type complexes has been observed before.[1, 2, 14] This is further corroborated by the 0.062 eV lower VIE of K(24-Crown-8) compared to the Na(24-Crown-8). The VIEs decrease in the order of M(9-Crown-3)$_2$ > M[2.1.1]Cryptand > M(3^{6}Adz) > M(*o*-Me$_2$-1.1.1) for M = Li and it is inversely correlated to the number of H-atoms in the solvation shells except for the M(3^{6}Adz) (Table 1). On the other hand, VIE vary in the order of M[2.1.1]Cryptand > M(9-Crown-3)$_2$ > Na(*o*-Me$_2$-1.1.1) > M(24-Crown-8) for M = Na. Similar to the M = Li case, the VIEs inversely correlate with the number of H-atoms of the complex, except for the Na[2.1.1]Cryptand.

To evaluate a potential relationship between VIE vs. the number of H-atoms in the solvation shell, literature EPT VIEs of similar Li- and Na-based Rydberg-type complexes were collected, and a plot was produced including the EPT VIEs of the molecules pursued in the present work (ESI Figure S3). The literature VIEs and the corresponding references are listed in the ESI Table S31. Clearly, the relationship between the VIEs vs. the number of H-atoms is negative for Li- and Na-complexes, but the correlations are moderate, i.e., the R^2 values of Li- and Na-complexes are 0.65 and 0.67,

respectively. Indeed, the VIEs of these complexes are expected to decrease with the expansion of the electron cloud and hence we expect larger diffuse complexes to possess smaller VIEs. Hence, a better relationship to pursue would be the VIE vs. $\Sigma r_{(M\cdots H)}$ in which the latter is related to the size of the molecule and the total number of H-atoms in the solvation shell. Hence, VIE vs. $\Sigma r_{(M\cdots H)}$ plots of Li- and Na-complexes are constructed and given in ESI Figure S4. As expected, the aforementioned relationship is negative with R^2 values of 0.72 and 0.65 for Li- and Na-complexes, respectively. Notice that the correlation is slightly improved in VIE vs. $\Sigma r_{(M\cdots H)}$ case for M = Li but declined for M = Na, compared to the corresponding relationships of VIE vs. the total number of H-atoms.

Table 1. Point group symmetries, CAM-B3LYP dissociation energies with respect to $M(L)_n \rightarrow M + nL$ fragmentation (D_e, kcal/mol), and EPT vertical ionization energies (VIE, eV) of $M(L)_n$ (M = Li, Na, K; n = 1, 2) systems.

Structure	Point group	D_e	VIE		
			D2	P3	P3+
Li(9-Crown-3)	C_3	18.4	2.950	2.943	2.944
Na(9-Crown-3)	C_3	7.9	3.250	3.246	3.246
Li(9-Crown-3)$_2$	S_6	36.8	1.893	1.902	1.901
Na(9-Crown-3)$_2$	S_6	11.3	1.839	1.848	1.847
Li[2.1.1]Cryptand	C_2	41.9	1.868	1.875	1.874
Na[2.1.1]Cryptand	C_2	10.5	1.859	1.866	1.865
Li(*o*-Me$_2$-1.1.1)	C_{3h}	24.7	1.722		
Na(*o*-Me$_2$-1.1.1)	C_{3h}	19.3	1.723		
Na(24-Crown-8)	S_4	16.8	1.731		
K(24-Crown-8)	S_4	13.0	1.669		
Li(3^6Adz)	S_4	35.9	1.865		

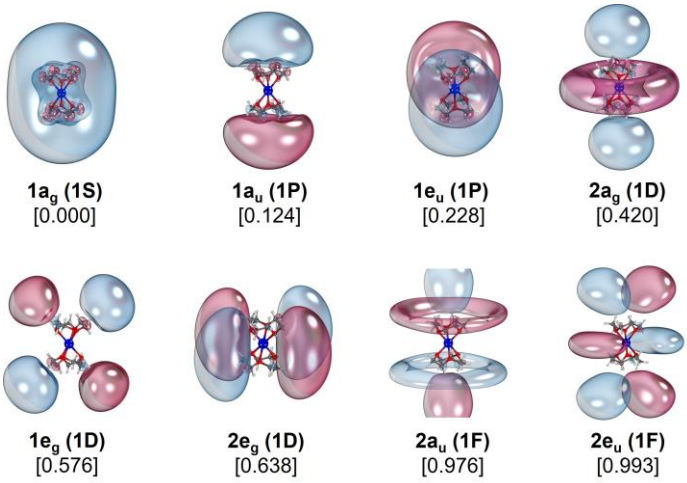

Figure 2. Molecular orbitals for several vertical electron attachments of Li(9-Crown-3)$_2$$^+$. A threshold of 70% was applied for orbital plots. The near SA shell notation is listed in parenthesis and P3+ vertical excitation energies (eV) are given in square brackets.

The excited state analysis of the Rydberg-type complexes is challenging due to the dependance of the accuracy of excitation energies on the level of theory and the basis set.[23, 26, 28, 29, 33] Highly expensive EOM-EA-CCSD (equation-of-motion coupled cluster singles and doubles method of electron attachment), CASPT2 (complete active space second-order perturbation theory), and EPT levels are known to provide highly accurate results on such species (see Refs. 24, 25, 33). On the other hand, the chosen basis set must be able to represent the highly diffuse electron cloud. According to our previous studies the cc-pVXZ (C, N, O, M = metal) d-aug-cc-pVXZ (H) combination is suitable for calculating accurate excitation energies (X = D or T) for such complexes.[1, 23, 25] Hence, in the present work the less expensive double-ζ quality (X = D) set was implemented with KT, D2, P3, and P3+ levels of EPT.

The molecules with expanded quasispherical (s-type) electron clouds (in the ground state) tend to populate p-, d-, f-, and g-type molecular orbitals (or P-, D-, F-, and G-SA orbitals) in excited states.[59] Similarly, all the reported surface-type complexes of this work populate SA orbitals in excited states. For example, some of those of the Li(9-Crown-3)$_2$ and the P3+ VIEs are given in the Figure 2. The excited states of both Li(9-Crown-3)$_2$ and Na(9-Crown-3)$_2$ are studied at KT, D2, P3, and P3+ levels and are listed in the Table 2. Under all four levels of theory, the observed SA order of both complexes is identical to the 1S, 1P, 1D, 1F, 2S, 2P, 2D, and 1G, except for the stabilization of 1G over the 2D at the KT. To shed some light on the origination of this shell model here, the lowest unoccupied orbitals (LUOs) of (9-crown-3)$_2$ obtained at the geometry of Li(9-crown-3)$_2$ were plotted (ESI Figure

S5). One can observe that all LUOs are diffuse in nature and the LUO and LUO+1 to LUO+3 mimic SA-1S and SA-1P orbitals, respectively. Similarly, LUO+4 to LUO+8 resemble SA-1D contours. The LUOs which mimic SA-1S of each [2.1.1]Cryptand, *o*-Me_2-1.1.1, 24-Crown-8, and 3^6Adz ligands are also plotted using the structures of their corresponding Na-complexes and are depicted in the ESI Figure S6. It should be noted that the idea of using LUOs to explain the populating orbital pattern has been reported before by Zurek et al., for metal ammonia complexes.[60]

The 1S → 1D, 1S → 1F, and 1S → 1G transition energies of all complexes and the 1S → 1P transition energy of M[2.1.1]Cryptand are listed as ranges in Table 2 for simplicity (see ESI Tables S12, S14, S16, S18, S20, S22, S24, S26, and S28 for all calculated VEEs). All excitation energies of Na(9-Crown-3)$_2$ are slightly lower compared to the Li(9-Crown-3)$_2$ (by 0-0.8 eV) except for the 1F (4^2A_u) and 2P (5^2A_u) which are higher by 0.005 and 0.093 eV, respectively (compare P3+ values of ESI Tables S12 and S14). The excited state analysis is carried out up to the 1F level for all other complexes (Table 2). The KT, D2, P3, and P3+ EPT levels are also tabulated for the M[2.1.1]Cryptand. For these complexes, i.e., M(9-Crown-3)$_2$ and M[2.1.1]Cryptand, the discrepancies between P3+ vs. P3, P3+ vs. D2, and P3+ vs. KT are less than 0.01, 0.02, and 0.21 eV, respectively. Due to the computational challenges, the excitation energies of the M(*o*-Me_2-1.1.1), M(24-Crown-8), and M(3^6Adz) complexes were calculated only at the D2 level of theory. Upon comparison of average 1S → 1P, 1S → 1D, and 1S → 1F transition energies at D2 level (ESI Table S30), all Na-complexes bear slightly lower VEEs compared to their Li-complexes (the differences are less than 0.01, 0.03, and 0.05 eV, respectively), except for M(*o*-Me_2-1.1.1) in which the Na-complex carries slightly higher VEEs (by ~0.002 eV for all transitions). On the other hand, as expected the K([24]Crown-8) has lower average VEEs compared to the Na([24]Crown-8) by 0.02, 0.03, and 0.05 eV for the aforementioned three transitions.

Table 2. Vertical excitation energies (VEEs, eV) of M(9-Crown-3)$_2$, M[2.1.1]Cryptand, M(*o*-Me_2-1.1.1), M(24-Crown-8), M(3^6Adz) (M = Li, Na, K) at EPT.

Approximate SA shell	KT	D2	P3	P3+
	Li(9-Crown-3)$_2$			
1S	0.000	0.000	0.000	0.000
1P[a]	0.122, 0.191	0.123, 0.229	0.125, 0.228	0.124, 0.228
1D	0.396–0.538	0.416–0.638	0.421–0.639	0.420–0.638
1F	0.851–0.978	0.973–1.126	0.977–1.131	0.976–1.130
2S	1.041	1.103	1.111	1.110
2P[a]	1.163, 1.347	1.228, 1.308	1.234, 1.318	1.233, 1.317
2D	1.500–1.741	1.408–1.715	1.423–1.717	1.421–1.717
1G[b]	1.296–1.325	1.484–1.525	1.489–1.529	1.488–1.529
	Na(9-Crown-3)$_2$			
1S	0.000	0.000	0.000	0.000

1P[a]	0.118, 0.180	0.120, 0.216	0.122, 0.215	0.122, 0.215
1D	0.354–0.526	0.358–0.627	0.363–0.626	0.362–0.626
1F	0.799–1.002	0.907–1.131	0.910–1.135	0.910–1.135
2S	1.014	1.067	1.074	1.074
2P[a]	1.148, 1.471	1.202, 1.400	1.207, 1.411	1.207, 1.410
2D	1.465–1.742	1.348–1.706	1.364–1.707	1.363–1.707
1G[b]	1.237–1.282	1.411–1.470	1.416–1.475	1.416–1.475
		Li[2.1.1]Cryptand		
1S	0.000	0.000	0.000	0.000
1P	0.136–0.198	0.148–0.248	0.149–0.245	0.148–0.245
1D	0.452–0.502	0.532–0.603	0.530–0.602	0.530–0.601
1F	0.824–0.895	0.953–1.057	0.954–1.057	0.953–1.057
		Na[2.1.1]Cryptand		
1S	0.000	0.000	0.000	0.000
1P	0.131–0.199	0.144–0.252	0.144–0.250	0.144–0.250
1D	0.442–0.504	0.521–0.608	0.519–0.607	0.519–0.607
1F	0.811–0.893	0.939–1.055	0.939–1.056	0.938–1.055
		Li(*o*-Me_2-1.1.1)		
1S		0.000		
1P[a]		0.153, 0.181		
1D		0.459–0.515		
1F		0.866–0.934		
		Na(*o*-Me_2-1.1.1)		
1S		0.000		
1P[a]		0.168, 0.187		
1D		0.473–0.503		
1F		0.858–0.930		
		Na(24-Crown-8)		
1S		0.000		
1P[a]		0.149, 0.203		
1D		0.403–0.507		
1F		0.842–0.917		
		K(24-Crown-8)		
1S		0.000		
1P[a]		0.139, 0.171		
1D		0.370–0.468		
1F		0.791–0.883		
		Li[3^6Adz]		
1S		0.000		
1P[a]		0.143, 0.153		
1D		0.516–0.566		
1F		0.949–0.995		

[a] Only two VEEs of each P^1 configuration are listed because of the degeneracies. [b] Within the focused energy range only three components of $1G^1$ (3^2E_g, 4^2E_g, 5^2A_g) were observed for Li(9-Crown-3)$_2$ and Na(9-Crown-3)$_2$ (ESI Tables S12 and S14). See ESI Tables S12, S14, S16, S18, S20, S22, S24, S26, and S28 for all calculated excitation energies, degeneracies, and corresponding orbitals.

III.B. DFT analysis

To accelerate the progression of studies on Rydberg-type systems, in the past we have performed a DFT benchmark study and identified the CAM-B3LYP functional to provide comparable structural parameters to the gold-standard CCSD(T).[30] To further expedite the analysis of such complexes, a part of this work is devoted for DFT benchmarking of ionization potentials and excitation energies. In this regard the VIEs were obtained for the Li(9-Crown-3)$_2$ with a series of functionals that span multiple rungs of Jacob's ladder and compared with the P3+ EPT value. Specifically, GGA (BP86[61, 62], BLYP[63, 64], PBE[65]), meta-GGA (TPSS[66], MN15-L[67]), global GGA hybrid (B3LYP[68-70], B3P86[61, 68], B3PW91[68, 71], PBE0[72]), meta-GGA hybrid (TPSSh[66], M06[73], M06-2X[73], MN15[74]), range-separated hybrid (LRC-ωPBE[75], CAM-B3LYP[76], ωB97X[77]), and double hybrid (PBE0-DH[78], DSDPBEP86[79, 80]) functionals were applied (Figure 3). The largest deviations from the P3+ VIE were observed for the cheaper GGAs with 19-25% errors. The meta-GGAs and global GGA hybrids predicted VIEs with 10-18% errors. The B3P86 VIE is not included in Figure 3 due to a convergence problem. The best set of functionals as a family is clearly the meta-GGA hybrids. Specifically, the errors of all M06, M06-2X, and MN15 are less than 5%, but the TPSSh carries ~11% error. Among range-separated hybrids, the LRC-ωPBE and CAM-B3LYP predicted better VIEs compared to the ωB97X. Obviously the DFT errors are minor (less than 4%) for the more expensive PBE0-DH and DSDPBEP86 double hybrids functionals. Among the chosen functionals all overestimated the VIEs compared to the P3+ except for the LRC-ωPBE, ωB97X, and DSDPBEP86. Overall, the VIEs of Li(9-Crown-3)$_2$ improved moving from GGA to double hybrid functionals demonstrating our general expectation, which is that the accuracy improves when moving to higher rungs of Jacob's ladder of density functional approximations.

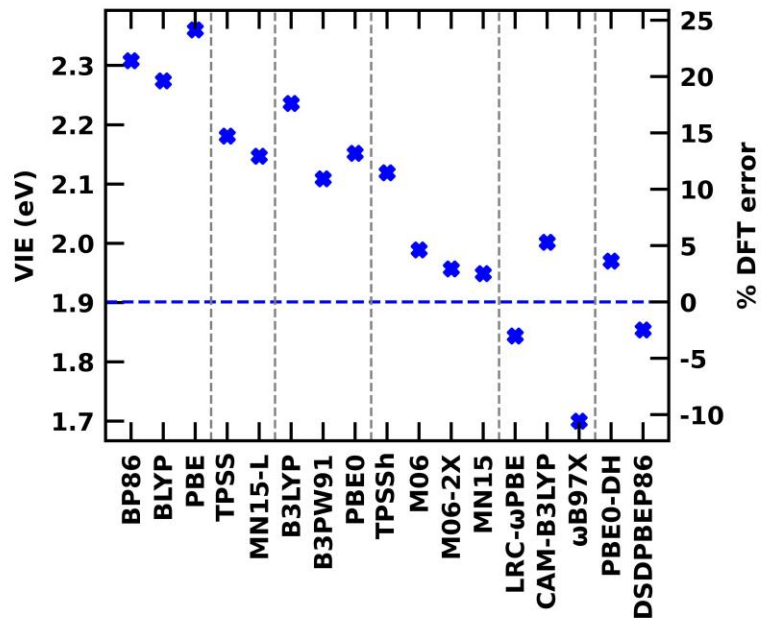

Figure 3. Vertical ionization energy (VIE, eV) of Li(9-Crown-3)$_2$ calculated with various exchange-correlation functionals at the cc-pVDZ (Li, C, O) d-aug-cc-pVDZ (H) basis set (blue cross marks). Each family of density functionals is separated with vertical gray lines and ordered by the rung on Jacob's ladder (left to right: GGA, meta-GGA, global GGA hybrid, meta-GGA hybrid, range-separated hybrid, and double hybrid). The horizontal blue dashed line represents the P3+ VIE of Li(9-Crown-3)$_2$. The % DFT errors are calculated with respect to the P3+ VIE.

The highly expensive excited state calculations are not feasible or carry challenges for larger complexes and the application of an appropriate TD-DFT method could be an alternative. Especially, the ease of use of TD-DFT could promote further studies on such complexes. Hence, next, we paid our attention towards the TD-DFT VEEs of the Li(9-Crown-3)$_2$. For TD-DFT calculations the same set of families of DFT mentioned earlier was applied except for the double hybrids (Figure 4). In some cases, the convergence issues were observed and results of those functionals are not included in the Figure 4. All functionals overestimated the 1S → 1P VEE except for the MN15 and many at the higher rungs performed well with minor discrepancies with respect to the P3+ (Figure 4). The largest errors compared to the P3+ were observed for the two GGA functionals, i.e., BLYP and PBE. The best description for this transition is clearly from the CAM-B3LYP with an almost identical value to the P3+ (0.198 vs. 0.193 eV). Interestingly, all the functionals predicted rather accurate 1S → 1D VEE except for the M06-2X and LRC-ωPBE which carry ~23% errors (others have less than 11% errors). The average 1S → 1F and 1S → 2S transition energies are only 0.065 eV apart from each other at the

P3+ level and all functionals beside the PBE, predicted the correct order (see the red and gray cross marks in Figure 4). For these transitions, larger errors were observed for the M06-2X, MN15, and LRC-ωPBE, but they are less than 15%. Upon consideration of all the VEEs the CAM-B3LYP functional is indeed in better agreement with the P3+ with minimal errors compared to the others. Specifically, its errors of 1S → 1P, 1S → 1D, 1S → 1F, and 1S → 2S VEEs are as small as 2.4, 5.2, 4.5, and 0.1%, respectively.

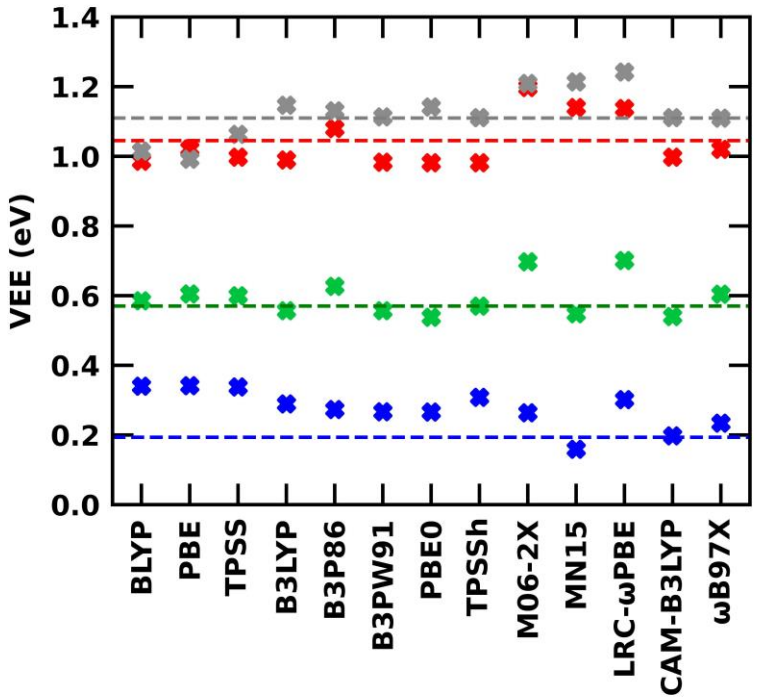

Figure 4. TD-DFT average vertical excitation energies (VEE, eV) of Li(9-Crown-3)$_2$ calculated with various exchange-correlation functionals at the cc-pVDZ (Li, C, O) d-aug-cc-pVDZ (H) basis set. The blue, green, red, and gray cross marks represent average vertical excitation energies correspond to the 1S → 1P, 1S → 1D, 1S → 1F, and 1S → 2S transitions, respectively. Similarly, the blue, green, red, and gray horizontal dashed lines represent the corresponding average P3+ VEEs, respectively.

Since CAM-B3LYP is the better choice for predicting both VIE and VEEs of Li(9-Crown-3)$_2$ its accuracy and transferability were tested for all other Rydberg-type species pursued in the present work and a few more such complexes reported in the literature. Specifically, the structures of M(NH$_3$)$_4$, M(en)$_2$, M(12-Crown-4), M(15-Crown-5), M(18-Crown-6), M([9]aneN$_3$)$_2$, M[18]aneN$_6$,

M[1.1.1]cryptand, M[2.2.2]cryptand, $M(Tren)_2$, M(Azacryptand), and M(TriPip222) of M = Li/Na/K collected from literature were used for DFT/CAM-B3LYP calculations. Note that the *ab initio* EPT (D2/P3+) VIE and/or VEE are already found for these selected complexes in the literature. The calculated DFT/CAM-B3LYP VIEs, average 1S → 1P and 1S → 1D VEEs, corresponding D2/P3+ EPT literature values, and corresponding references are listed in the ESI Tables S31 and S32. The CAM-B3LYP vs. EPT VIEs of complexes are plotted and given in the Figure 5a. Notice that their relationship is as linear as $R^2 = 0.99$. The average 1S → 1P and 1S → 1D VEEs provided by the two techniques are depicted in the Figures 5b and 5c and in both cases the linearity is $R^2 = 0.98$. Note that these plots can be used to predict highly accurate VIE or VEEs for similar complexes with the use of DFT/CAM-B3LYP values. For example, DFT/CAM-B3LYP VIEs and VEEs were computed for the $K([10]aneN_4)_2$, K[2.2.2]Cryptand, and hexa-methylated and hexa-ethylated complexes of K[2.2.2]Cryptand (see ESI Figure S7) and extrapolated to evaluate the corresponding EPT values. Specifically, the purple, light-blue, brown, and red colored extrapolated arrows of a, b, and c plots of Figure 5 correspond to the $K([10]aneN_4)_2$, K[2.2.2]Cryptand, hexa-methylated-K[2.2.2]Cryptand, and hexa-ethylated-K[2.2.2]Cryptand complexes, respectively. The CAM-B3LYP vs. the predicted-EPT VIEs of these four complexes are 2.067 vs. 1.943, 1.751 vs. 1.658, 1.621 vs. 1.542, and 1.579 vs. 1.503 eV, respectively. The 1S → 1P VEEs of these complexes are 0.264 vs. 0.245, 0.127 vs. 0.123, 0.051 vs. 0.055, 0.089 vs. 0.088 eV, respectively. Similarly, those of the 1S → 1D are 0.689 vs. 0.675, 0.392 vs. 0.400, 0.317 vs. 0.330, 0.350 vs. 0.361 eV.

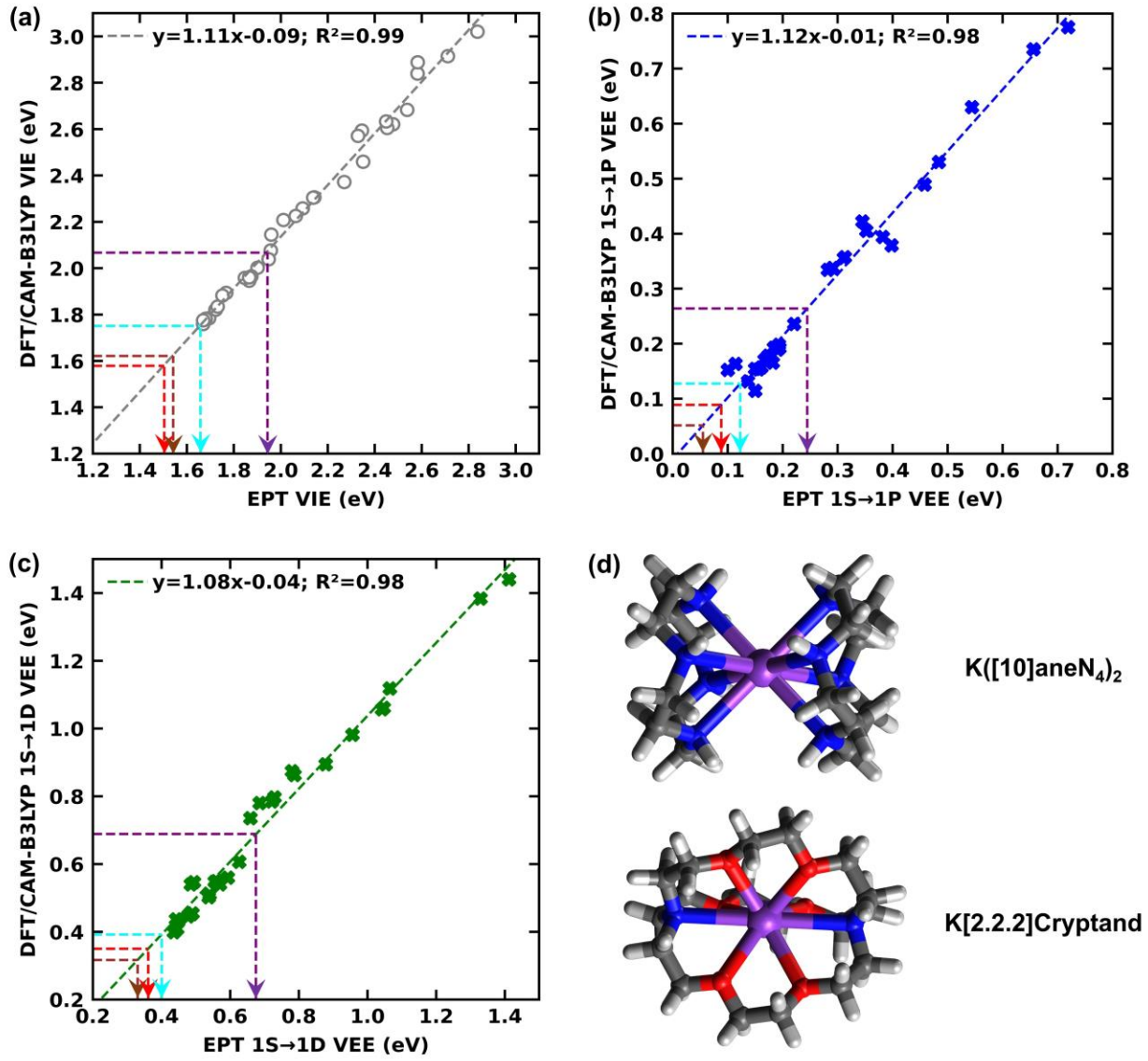

Figure 5. (a) DFT/CAM-B3LYP vertical ionization energy (VIE) vs. corresponding D2/P3+ EPT VIE (open gray circles), (b) DFT/CAM-B3LYP 1S → 1P vertical excitation energy (VEE) vs. corresponding D2/P3+ EPT 1S → 1P VEE (blue cross marks), (c) DFT/CAM-B3LYP 1S → 1D VEE vs. corresponding D2/P3+ EPT 1S → 1D VEE (green cross marks) of complexes with diffuse electrons. All values are in eV (the numerical values are listed in ESI Tables S31 and S32). (d) Geometries of K([10]aneN$_4$)$_2$ and K[2.2.2]Cryptand complexes. Purple and cyan colored extrapolated arrows of a, b, and c plots represent the VIEs or VEEs of K([10]aneN$_4$)$_2$ and K[2.2.2]Cryptand complexes. The brown and red colored arrows of the plots correspond to the methylated- and ethylated-K[2.2.2]Cryptand complexes, respectively.

IV. Conclusions

The knowledge progression of Rydberg-type systems has always been lagging due to their complicated electronic structures and the high-level of quantum chemical expertise required for their analysis. With the intention of exploring and appreciating their chemistries, we investigated here a series of such complexes. Specifically, electronic structure calculations are executed to analyze ground and excited states of M(9-Crown-3)$_2$, M[2.1.1]Cryptand, M(*o*-Me$_2$-1.1.1), M(24-Crown-8), and M(3^6Adz) complexes (M = Li/Na/K). The ground state of each of these complexes carries an electron in a diffuse quasispherical s-type (or SA-1S) orbital. These solvated complexes bear smaller ionization potentials than any atom in the periodic table and hence belong to the superalkali category. The lowest ionization energy was observed for the larger K(24-Crown-8) complex, i.e., 1.669 eV. In excited states these complexes populate SA-1P, -1D, -1F orbitals and can be recognized as superatoms. The M(9-Crown-3)$_2$ complexes carry the 1S, 1P, 1D, 1F, 2S, 2P, 2D, 1G shell model, and the occupying SA orbitals are analogous to the LUOs of (9-crown-3)$_2$ collected at Li(9-crown-3)$_2$ geometry.

To expedite the progression on studies of Rydberg or similar complexes, a DFT benchmark case study was conducted for VIE and VEEs of Li(9-Crown-3)$_2$ using EPT/P3+ data as reference values. For DFT calculations a series of functionals that belong to the GGA, meta-GGA, global GGA hybrid, meta-GGA hybrid, range-separated hybrid, and double hybrid families were used. The DFT VIE predictions systematically improved when moving to higher rungs of Jacob's ladder, which indeed was our expectation. Overall, functionals of meta-GGA hybrids, range-separated hybrids, and double hybrids predicted VIEs with minor errors (less than 6%), except for TPSSh and ωB97X for which the errors are ~11%. The best functional for predicting all 1S → 1P, 1S → 1D, 1S → 1F, and 1S → 2S transitions is the range-separated hybrid CAM-B3LYP and the errors are less than 6%. The accuracy of CAM-B3LYP on VIE and VEEs was further tested using similar Rydberg-type complexes reported in the literature, where strong correlations were observed between DFT/CAM-B3LYP vs. EPT and the introduced relationships are convenient for predicting more accurate VIE and VEEs of similar systems. Finally, we believe more DFT functional error analysis on multi-Rydberg-electron complexes, transition metal-based Rydberg-type complexes, and less symmetric/distorted Rydberg-type systems are vital on gaining further information on DFT applicability on them, which could further accelerate the progression of this filed of science.

Acknowledgements

The support of the Los Alamos National Laboratory (LANL) Laboratory Directed Research and Development program Project No. 20240737PRD1 is acknowledged. This research used resources

provided by the Los Alamos National Laboratory Institutional Computing Program, which is supported by the U.S. Department of Energy National Nuclear Security Administration under Contract No. 89233218CNA000001. Prof. Michael McKee is thanked for his useful comments on improving this work.

Conflicts of interest

There are no conflicts to declare.

Electronic supplementary information (ESI) available

Tables S1-S7 list the Cartesian coordinates of optimized geometries; Tables S8-S11 list the harmonic vibrational frequencies of the geometries; Tables S12, S14, S16, S18, S20, S22, S24, S26, and S28 list VEEs of studied molecules; Tables S13, S15, S17, S19, S21, S23, S25, S27, and S29 list VEAEs and corresponding PS values of cationic complexes; Table S30 lists bond lengths and average VEEs of studied complexes, Table S31 lists VIEs and average VEEs of a series of Rydberg-type complexes available in the literature; Table S32 lists the CAM-B3LYP VIEs and average VEEs of a series of Rydberg-type complexes available in the literature; Figure S1 illustrates the contours of singly occupied molecular orbitals of studied complexes; Figure S2 illustrates the geometries of Li(*o*-Me_2-1.1.1); Figure S3 and S4 illustrate the variation of the VIE vs. the number of H-atoms or $\Sigma r_{(M\cdots H)}$; Figures S5 and S6 illustrate the LUOs of chelating ligands; Figure S7 illustrates the geometries of the studied three large cryptand complexes.

References

1. I. R. Ariyarathna, *International Journal of Quantum Chemistry*, 2021, **121**.
2. I. R. Ariyarathna, *Phys Chem Chem Phys*, 2021, **23**, 18588-18594.
3. X. Wang, J. Feng, Y. Bai, Q. Zhang and Y. Yin, *Chem Rev*, 2016, **116**, 10983-11060.
4. N. V. Tkachenko, P. Rublev, A. I. Boldyrev and J. M. Lehn, *Front Chem*, 2022, **10**, 880804.
5. G. Monta-Gonzalez, F. Sancenon, R. Martinez-Manez and V. Marti-Centelles, *Chem Rev*, 2022, **122**, 13636-13708.
6. X. Yang, Z. Ullah, J. F. Stoddart and C. T. Yavuz, *Chem Rev*, 2023, **123**, 4602-4634.
7. R. Ham, C. J. Nielsen, S. Pullen and J. N. H. Reek, *Chem Rev*, 2023, **123**, 5225-5261.
8. B. D. Nath, K. Takaishi and T. Ema, *Catalysis Science & Technology*, 2020, **10**, 12-34.
9. M. Yadav, D. Yadav, D. Pal Singh and J. Kumar Kapoor, *Inorganica Chimica Acta*, 2023, **546**.
10. N. A. Thiele, J. J. Woods and J. J. Wilson, *Inorg Chem*, 2019, **58**, 10483-10500.
11. Y. Z. Voloshin and A. S. Belov, *Russian Chemical Reviews*, 2008, **77**, 161-175.
12. F. A. Cotton and G. Wilkinson, *Advanced Inorganic Chemistry*, John wiley and sons, New York, 4th edn., 1980.

13. Z. Lu, B. A. Jackson and E. Miliordos, *Molecules*, 2023, **28**.
14. N. V. Tkachenko, Z. M. Sun and A. I. Boldyrev, *Chemphyschem*, 2019, **20**, 2060-2062.
15. I. R. Ariyarathna, *Inorg Chem*, 2022, **61**, 579-585.
16. I. R. Ariyarathna and E. Miliordos, *Phys Chem Chem Phys*, 2021, **23**, 20298-20306.
17. G. L. Gutsev and A. I. Boldyrev, *Chemical Physics Letters*, 1982, **92**, 262-266.
18. B. A. Jackson, S. G. Dale, M. Camarasa-Gómez and E. Miliordos, *The Journal of Physical Chemistry C*, 2023, **127**, 9295-9308.
19. B. A. Jackson and E. Miliordos, *Chem Commun (Camb)*, 2022, **58**, 1310-1313.
20. I. R. Ariyarathna, *J Comput Chem*, 2024, **45**, 655-662.
21. B. K. Teo and S.-Y. Yang, *Journal of Cluster Science*, 2015, **26**, 1923-1941.
22. I. R. Ariyarathna, F. Pawlowski, J. V. Ortiz and E. Miliordos, *Phys Chem Chem Phys*, 2018, **20**, 24186-24191.
23. I. R. Ariyarathna, S. N. Khan, F. Pawlowski, J. V. Ortiz and E. Miliordos, *J Phys Chem Lett*, 2018, **9**, 84-88.
24. I. R. Ariyarathna and E. Miliordos, *Phys Chem Chem Phys*, 2020, **22**, 22426-22435.
25. I. R. Ariyarathna and E. Miliordos, *Phys Chem Chem Phys*, 2019, **21**, 15861-15870.
26. S. N. Khan and E. Miliordos, *J Phys Chem A*, 2020, **124**, 4400-4412.
27. I. R. Ariyarathna, N. M. S. Almeida and E. Miliordos, *J Phys Chem A*, 2019, **123**, 6744-6750.
28. N. M. S. Almeida and E. Miliordos, *Phys Chem Chem Phys*, 2019, **21**, 7098-7104.
29. N. M. S. Almeida, F. Pawlowski, J. V. Ortiz and E. Miliordos, *Phys Chem Chem Phys*, 2019, **21**, 7090-7097.
30. I. R. Ariyarathna, F. Pawlowski, J. V. Ortiz and E. Miliordos, *J Phys Chem A*, 2020, **124**, 505-512.
31. J. V. Ortiz, I. Martin, A. M. Velasco and C. Lavin, *J Chem Phys*, 2004, **120**, 7949-7954.
32. H. Reisler and A. I. Krylov, *International Reviews in Physical Chemistry*, 2009, **28**, 267-308.
33. I. R. Ariyarathna, *Phys Chem Chem Phys*, 2021, **23**, 16206-16212.
34. K. Sambe, N. Hoshino, T. Takeda, T. Nakamura and T. Akutagawa, *Crystal Growth & Design*, 2020, **20**, 3625-3634.
35. A. Ahsan, S. Sarfaraz, F. Fayyaz, M. Asghar and K. Ayub, *Materials Science in Semiconductor Processing*, 2023, **153**.
36. W.-M. Sun, X. Cheng, Y.-L. Ye, X.-H. Li and B.-L. Ni, *Organometallics*, 2022, **41**, 412-417.
37. Z.-J. Zhou, H. Li, X.-R. Huang, Z.-J. Wu, F. Ma and Z.-R. Li, *Computational and Theoretical Chemistry*, 2013, **1023**, 99-103.
38. S. Cantrill, *Nature Chemistry*, 2015, **7**, 536-536.
39. R. C. Brachvogel, H. Maid and M. von Delius, *Int J Mol Sci*, 2015, **16**, 20641-20656.
40. R. C. Brachvogel, F. Hampel and M. von Delius, *Nat Commun*, 2015, **6**, 7129.
41. R. Rencsok, T. A. Kaplan and J. F. Harrison, *The Journal of Chemical Physics*, 1993, **98**, 9758-9764.
42. J. P. Perdew, presented in part at the AIP Conference Proceedings, 2001.
43. B. P. Prascher, D. E. Woon, K. A. Peterson, T. H. Dunning and A. K. Wilson, *Theoretical Chemistry Accounts*, 2010, **128**, 69-82.
44. J. G. Hill and K. A. Peterson, *J Chem Phys*, 2017, **147**, 244106.
45. R. A. Kendall, T. H. Dunning and R. J. Harrison, *The Journal of Chemical Physics*, 1992, **96**, 6796-6806.
46. T. H. Dunning, *The Journal of Chemical Physics*, 1989, **90**, 1007-1023.
47. T. Koopmans, *Physica*, 1934, **1**, 104-113.
48. Y. Ö. Jan Linderberg, *Propagators in Quantum Chemistry*, John Wiley & Sons, New Jersey, 2004.
49. J. V. Ortiz, *International Journal of Quantum Chemistry*, 2005, **105**, 803-808.
50. J. V. Ortiz, *WIREs Computational Molecular Science*, 2012, **3**, 123-142.
51. H. H. Corzo and J. V. Ortiz, in *Löwdin Volume*, 2017, Advances in Quantum Chemistry, pp. 267-298.

52. M. J. Frisch, G. W. Trucks, H. B. Schlegel, G. E. Scuseria, M. A. Robb, J. R. Cheeseman, G. Scalmani, V. Barone, G. A. Petersson, H. Nakatsuji, X. Li, M. Caricato, A. V. Marenich, J. Bloino, B. G. Janesko, R. Gomperts, B. Mennucci, H. P. Hratchian, J. V. Ortiz, A. F. Izmaylov, J. L. Sonnenberg, Williams, F. Ding, F. Lipparini, F. Egidi, J. Goings, B. Peng, A. Petrone, T. Henderson, D. Ranasinghe, V. G. Zakrzewski, J. Gao, N. Rega, G. Zheng, W. Liang, M. Hada, M. Ehara, K. Toyota, R. Fukuda, J. Hasegawa, M. Ishida, T. Nakajima, Y. Honda, O. Kitao, H. Nakai, T. Vreven, K. Throssell, J. A. Montgomery Jr., J. E. Peralta, F. Ogliaro, M. J. Bearpark, J. J. Heyd, E. N. Brothers, K. N. Kudin, V. N. Staroverov, T. A. Keith, R. Kobayashi, J. Normand, K. Raghavachari, A. P. Rendell, J. C. Burant, S. S. Iyengar, J. Tomasi, M. Cossi, J. M. Millam, M. Klene, C. Adamo, R. Cammi, J. W. Ochterski, R. L. Martin, K. Morokuma, O. Farkas, J. B. Foresman and D. J. Fox, *Gaussian* 16, Wallingford CT 2016.
53. G. Knizia, *J Chem Theory Comput*, 2013, **9**, 4834-4843.
54. M. D. Hanwell, D. E. Curtis, D. C. Lonie, T. Vandermeersch, E. Zurek and G. R. Hutchison, *J. Cheminform.*, 2012, **4**, 17.
55. *Avogadro: an open-source molecular builder and visualization tool*, Version 1.2.0.
56. G. Schaftenaar and J. H. Noordik, *J Comput Aided Mol Des*, 2000, **14**, 123-134.
57. B. M. Reinhard and G. Niedner-Schatteburg, *Physical Chemistry Chemical Physics*, 2002, **4**, 1471-1477.
58. T. Tsurusawa and S. Iwata, *The Journal of Physical Chemistry A*, 1999, **103**, 6134-6141.
59. B. A. Jackson, S. N. Khan and E. Miliordos, *Chem Commun*, 2023, **59**, 10572-10587.
60. E. Zurek, P. P. Edwards and R. Hoffmann, *Angew Chem Int Ed Engl*, 2009, **48**, 8198-8232.
61. J. P. Perdew, *Phys. Rev. B Condens. Matter.*, 1986, **33**, 8822-8824.
62. A. D. Becke, *Phys. Rev. A Gen. Phys.*, 1988, **38**, 3098-3100.
63. B. Miehlich, A. Savin, H. Stoll and H. Preuss, *Chem. Phys. Lett.*, 1989, **157**, 200-206.
64. F. J. Devlin, J. W. Finley, P. J. Stephens and M. J. Frisch, *J. Phys. Chem.*, 1995, **99**, 16883-16902.
65. J. P. Perdew, K. Burke and M. Ernzerhof, *Phys. Rev. Lett.*, 1996, **77**, 3865-3868.
66. J. Tao, J. P. Perdew, V. N. Staroverov and G. E. Scuseria, *Phys. Rev. Lett.*, 2003, **91**, 146401.
67. H. S. Yu, X. He and D. G. Truhlar, *J. Chem. Theory Comput.*, 2016, **12**, 1280-1293.
68. A. D. Becke, *J. Chem. Phys.*, 1993, **98**, 5648-5652.
69. C. Lee, W. Yang and R. G. Parr, *Phys. Rev. B Condens. Matter.*, 1988, **37**, 785-789.
70. P. J. Stephens, F. J. Devlin, C. F. Chabalowski and M. J. Frisch, *J. Phys. Chem.*, 1994, **98**, 11623-11627.
71. J. P. Perdew, J. A. Chevary, S. H. Vosko, K. A. Jackson, M. R. Pederson, D. J. Singh and C. Fiolhais, *Phys. Rev. B Condens. Matter.*, 1992, **46**, 6671-6687.
72. C. Adamo and V. Barone, *J. Chem. Phys.*, 1999, **110**, 6158-6170.
73. Y. Zhao and D. G. Truhlar, *Theor. Chem. Acc.*, 2007, **120**, 215-241.
74. H. S. Yu, X. He, S. L. Li and D. G. Truhlar, *Chem. Sci.*, 2016, **7**, 5032-5051.
75. M. A. Rohrdanz, K. M. Martins and J. M. Herbert, *J. Chem. Phys.*, 2009, **130**, 054112.
76. T. Yanai, D. P. Tew and N. C. Handy, *Chem. Phys. Lett.*, 2004, **393**, 51-57.
77. J. D. Chai and M. Head-Gordon, *J Chem Phys*, 2008, **128**, 084106.
78. E. Bremond and C. Adamo, *J. Chem. Phys.*, 2011, **135**, 024106.
79. S. Kozuch and J. M. Martin, *Phys. Chem. Chem. Phys.*, 2011, **13**, 20104-20107.
80. S. Kozuch and J. M. Martin, *J. Comput. Chem.*, 2013, **34**, 2327-2344.